Comparing Poynting flux dominated with kinetic-energy dominated jets

M. Huarte-Espinosa[1], A. Frank[1], E. G. Blackman[1], A. Ciardi[2,3], P. Hartigan[4]

S. V. Lebedev[5]

Received _____; accepted _____

[1]Department of Physics and Astronomy, University of Rochester, 600 Wilson Boulevard, Rochester, NY, 14627-0171

[2]LERMA, Université Pierre et Marie Curie, Observatoire de Paris, Meudon, France

[3]École Normale Supérieure, Paris, France. UMR 8112 CNRS

[4]Rice University, Department of Physics and Astronomy, 6100 S. Main, Houston, TX 77521-1892

[5]The Blackett Laboratory, Imperial College London, SW7 2BW London, UK

ABSTRACT

Modern theoretical models of astrophysical jets combine accretion, rotation, and magnetic fields to launch and collimate supersonic flows from a central source. Near the source, magnetic field strengths must be large enough to collimate the jet, and for that to happen the Poynting flux must exceed the kinetic-energy flux of the jet in these regions. Stronger fields produce systems where the energy transport in the jet continues to be Poynting-flux-dominated (PFD) at larger distances as well. PFD jets recently created in laboratory experiments have provided important insights into these systems. In this paper we present 3-D radiative magnetohydrodynamical AMR simulations of PFD jets in order to (i) quantify how the propagation of PFD jets differs from that of their hydrodynamical (HD) counterparts, and (ii) compare how radiation, cooling, and rotation affect stability in PFD and HD jets. We find that PFD jets are lighter, slower, and less stable as compared to HD jets, characteristics that should be detectable observationally. Unlike HD jets, PFD jets develop current-driven perturbations that grwo faster as cooling and rotation increase, resulting in jets that are clumpier than those in the HD limit [true?].

Subject headings: ? — ? — ? —

1. Introduction

Non-relativistic jets are observed in the vicinities of many Protostellar Objects, Young Stellar Objects (YSOs) and post-AGB stars. In general the jets appear to be magnetized, collimated outflows which are dominated by the kinetic energy of the jet beam. Polarimetric measurements often find that jet magnetic fields have two main components: one parallel and one perpendicular to the beams (see e.g. Carrasco-González et al. 2010). Plausible models suggest that jets are launched and collimated by a symbiosis of accretion, rotation and magnetic mechanisms, which occur at the jet "central engine" (see Pudritz et al. 2007, for a review). Magnetic fields with initially poloidal (radial and vertical) dominant geometries anchored to accretion discs have been shown to form tall, highly wound and helical magnetic structures, or magnetic towers, that expand vertically when laterally supported in pressure equilibrium with the ambient gas (Lynden-Bell 1996, 2003). The jets' magnetic energy in expected to dominate over the kinetic energy close to the engines. Thus the relative strength of the jet magnetic field to the kinetic field seems to scale down with the distance from the engine. This process is unclear however in part because the resolution of telescopes is insufficient to directly observe the engines.

The relative extent over which magnetic energy dominates the outflow kinetic energy in a propagating jet has traditionally led to the definition of two outflow classes: magnetocentrifugal jets (Blandford & Payne 1982; Ouyed & Pudritz 1997; Blackman et al. 2001; Mohamed & Podsiadlowski 2007), in which magnetic fields only dominate out to the Alfvén radius, or Poynting flux dominated (PFD) jets (Lynden-Bell 1996; Ustyugova et al. 2000; Lovelace et al. 2002; Nakamura & Meier 2004) in which magnetic fields dominate the jet structure, acting as a magnetic piston over very large distances from the engine. PFD jets carry large electric currents which generate strong, tightly wound helical magnetic fields around the jet axis, **hence the synonym magnetic towers.**

Simulations of such jets have found that magnetic fields play a role in the formation of current-driven kink instabilities and the stabilization of Kelvin-Helmholtz (KH) modes in jets (e.g. see Nakamura & Meier 2004). While the correlation between the mechanical power of astrophysical jets and their main observable features (e.g. length, velocity, cocoon geometry, etc.) has been well characterized in the case of kinetic-energy dominated, or hydrodynamic, jets, this is not the case for magnetic towers.

Recently, magnetized jets have been produced in laboratory experiments which have successfully reproduced key aspects of magnetic tower evolution (Lebedev et al. 2005; Suzuki-Vidal et al. 2010). In these experiments, based on Pulsed Power current generators, the local injection of purely toroidal magnetic energy produced high Mach number ($M \sim 20$), fully radiative and fully magnetized jets. The dynamics of magnetic towers, represented by both a low β (thermal to magnetic pressure ratio) supersonically expanding cavity and a higher β jet, have been fully explored in these experiments providing new insights into their evolution. In particular, the stability properties of the central jets as well as the non-linear evolution of such instabilities have been characterized. The break-up of the jet into a sequence of collimated clumps has been suggestive as an explanation for clumpy flows observed in YSO outflow systems (Hartigan & Morse 2007, Yirak et al. 2010 (?) Hartigan et al. 2011). The experiments were also modeled via resistive MHD simulations developed for laboratory studies Ciardi et al. (2007) where the details of the flow, including current distributions, were followed.

Other critical factors for the stability of jets, in addition to the geometry and strength of their magnetic field, are strong thermal energy losses, in both the jet and the ambient materials, and rotation of the jet beam. A number of observations have found important cooling signatures in many jet environments (e.g. YSOs, **REF**) as well as jet beam radial velocity differences of order $10\,\mathrm{km\,s^{-1}}$ (see e.g. Bacciotti et al. 200). We note that

the effects of plasma cooling via optically thin radiation has been followed only in few simulations of magnetized, kinetic energy-dominated jets. These, have been found to form both thin cocoons and nose cones (e.g. Blondin et al. 1990; Frank et al. 1998), and to be more susceptible to KH instabilities relative to adiabatic jets (Hardee & Stone 1997, and references therein). In this paper we study the effect of radiative cooling and rotation on the stability of both magnetic towers and pre-collimated asymptotically hydrodynamic jets. We note that in practice the latter could represent the asymptotic propagation regimes of magneto-centrifugally launched jets, which are distinct from PFD in that PFD remain PFD out to much larger distances.

This paper is organized as follows: in section 2 we describe the methodology and numerical code that we use for this study as well as our implementation of the gas, the velocity and the magnetic field. The results of our simulations are presented in section 3, where we follow the evolution, structure and stability of our model jets. In section 4 we discuss the relevance of our simulations and how they compare with specific laboratory experiments on jets and observations of YSO and HH objects. Finally, our conclusions are presented in section 5.

2. Model

We model magnetic towers and a hydrodynamical jet using numerical simulations. This was done by solving the equations of magnetohydrodynamics (MHD) in three-dimensions, which in non-dimensional conservative form are given by

$$\frac{\partial \rho}{\partial t} + \nabla \cdot (\rho \mathbf{V}) = \dot{\rho}_{\rm inj} \tag{1}$$

$$\frac{\partial (\rho \mathbf{V})}{\partial t} + \nabla \cdot \left(\rho \mathbf{V}\mathbf{V}\,\hat{\mathbf{I}} + p + B^2/2 - \mathbf{B}\mathbf{B}\,\hat{\mathbf{I}} \right) = \dot{\mathbf{P}}_{\rm inj} \tag{2}$$

$$\frac{\partial E}{\partial t} + \nabla \cdot \left[\left(E + p + B^2/2\right)\mathbf{V} - \mathbf{B}(\mathbf{V}\cdot\mathbf{B})\right] = \dot{E}_{\rm inj} - \Delta(T) \quad (3)$$

$$\frac{\partial \mathbf{B}}{\partial t} - \nabla \times (\mathbf{V} \times \mathbf{B}) = \dot{\mathbf{B}}_{\rm inj}, \quad (4)$$

where ρ, p, **V, B** and $\hat{\rm I}$ are the gas density, thermal pressure, flow velocity, magnetic field and **the unitary tensor,** respectively. In (3), $E = p/(\gamma-1) + \rho V^2/2 + B^2/2$ and represents the total energy density whereas γ is the ratio of specific heats. We have implemented source terms in the right hand side of equations (1)–(4) to model the injection of mass, momentum, **total** energy and magnetic **flux,** which are given by $\dot{\rho}_{\rm inj}$, $\dot{\mathbf{P}}_{\rm inj}$, $\dot{E}_{\rm inj} - \Delta(T)$ and $\dot{\mathbf{B}}_{\rm inj}$, respectively. **The injection of energy has a kinetic, $\dot{E}_{\rm inj}$, and a cooling component which we will describe in section 2.3.**

We solve these equations using the adaptive mesh refinement (AMR) numerical code *AstroBEAR2.0*[1] which uses a second-order **unsplit** shock capturing scheme, a constrained transport method and Marquina flux functions (Cunningham et al. 2009; Carroll-Nellenback et al. 2011). While AstroBEAR2.0 is able to compute several microphysical processes, such as gas self-gravity and heat conduction, we do not consider these in the present study.

The computational domain we use is defined within $|x|, |y| \leq 160\,{\rm AU}$ and $0 \leq z \leq 400\,{\rm AU}$, where 20 AU are equivalent to one computational length unit. We use a coarse grid of $64\times64\times80$ cells plus two levels of AMR refinement which attain an effective resolution of 1.25 AU. Outflow boundary conditions were set at the left and right domain faces of both x and y, as well as in the upper z face. At the lower z face we combine two boundary conditions: reflective, in those cells located at $\sqrt{x^2+y^2} \geq r_e$, or magnetic/jet source term values, in those cells located at smaller radii. $r_e = 31.4\,{\rm AU}$ and represents the characteristic radius of the energy injection region, equal to the jets' radius, which is resolved by 24 cells.

[1]http://bearclaw.pas.rochester.edu/trac/astrobear/wiki

We use BlueGene/P[2], an IBM massively parallel processing supercomputer of the Center for Research Computing of the University of Rochester, to run simulations for about 1 day using 512 processors.

2.1. Initial conditions

We start our simulations with a static gas which has a constant density and temperature of 200 particles per cm^{-3} and 10000 K, respectively. Gas is modelled with an ideal gas equation of state and a ratio of specific heats of $\gamma = 5/3$. Magnetic fields are placed in a central cylinder of both radius and height r_e. In cylindrical coordinates the magnetic vector potential is given by

$$\mathbf{A}(r,z) = \begin{cases} \frac{r}{4}(cos(2\,r)+1)(cos(2\,z)+1)\hat{\phi} + \frac{\alpha}{8}(cos(2\,r)+1)(cos(2\,z)+1)\hat{k}, & \text{for } r,z < r_e; \\ 0, & \text{for } r,z \geq r_e, \end{cases} \tag{5}$$

where the parameter α has units of length and determines the ratio of toroidal to poloidal magnetic fluxes. We use $\alpha = 40$ (computational length units) which is an arbitrary choice, yet consistent with the highly wound helical magnetic configurations that are expected in accretion disk (e.g. Blandford & Payne 1982; Lynden-Bell 1996; Li et al. 2006) and produced in high energy density laboratory experiments of magnetic towers (Lebedev et al. 2005; Ciardi et al. 2007).

Our choice of $\mathbf{A}$ is in part motivated by the work of Li et al. (2006). However, in our model $\mathbf{A}$ is strictly localized to the central part of the grid. Then we obtain the initial

[2]https://www.rochester.edu/its/web/wiki/crc/index.php/Blue_Gene/P

magnetic field, $\mathbf{B}^{\rm init}$, by taking the curl of $\mathbf{A}$:

$$\begin{aligned} B_r^{\rm init} &= -\tfrac{\partial}{\partial z}(A_\phi) = 2rcos^2(r)cos(z)sin(z), \\ B_\phi^{\rm init} &= -\tfrac{\partial}{\partial r}(A_z) = \alpha cos^2(z)cos(r)sin(r), \\ B_z^{\rm init} &= \tfrac{1}{r}\tfrac{\partial}{\partial r}(rA_\phi) = 2cos^2(z)[cos^2(r) - rcos(r)sin(r)]. \end{aligned} \tag{6}$$

Finally, the magnetic field is normalized so that the parameter β, which is the ratio of the gas thermal pressure over the magnetic pressure, is less than 1 for $r < r_e$, and unity at $r = r_e$. In Figure 1 we show profiles of the magnetic field components (top and middle rows) and β (bottom panel) as a function the distance form the origin.

2.2. Energy injection

One of the motivations of this work is to compare Poynting flux dominated jets to hydrodynamic kinetic-energy dominated ones. In particular, we study their propagation and main observable features, e.g. their length, velocity, gas distribution, etc. To this end, we continually inject either magnetic **flux** or kinetic energy into the central region of the grid, $r, z \leq r_e$ (end of section 2).

2.2.1. Magnetic towers

For these simulations magnetic energy is injected by adding the initial magnetic field configuration (6) to the instantaneous central magnetic fields, $\mathbf{B}^n$. i.e.

$$\mathbf{B}^{n+1} = \mathbf{B}^n + \dot{\mathbf{B}}_{\rm inj}\, dt, \tag{7}$$

where $\mathbf{B}^{n+1}$ represents the central magnetic fields ($r, z \leq r_e$) corresponding to the next computational timestep, dt is the current timestep, $\dot{\mathbf{B}}_{\rm inj} = \mathbf{B}^{\rm init}\, B_c$ and B_c is the magnetic **flux** injection rate (see below).

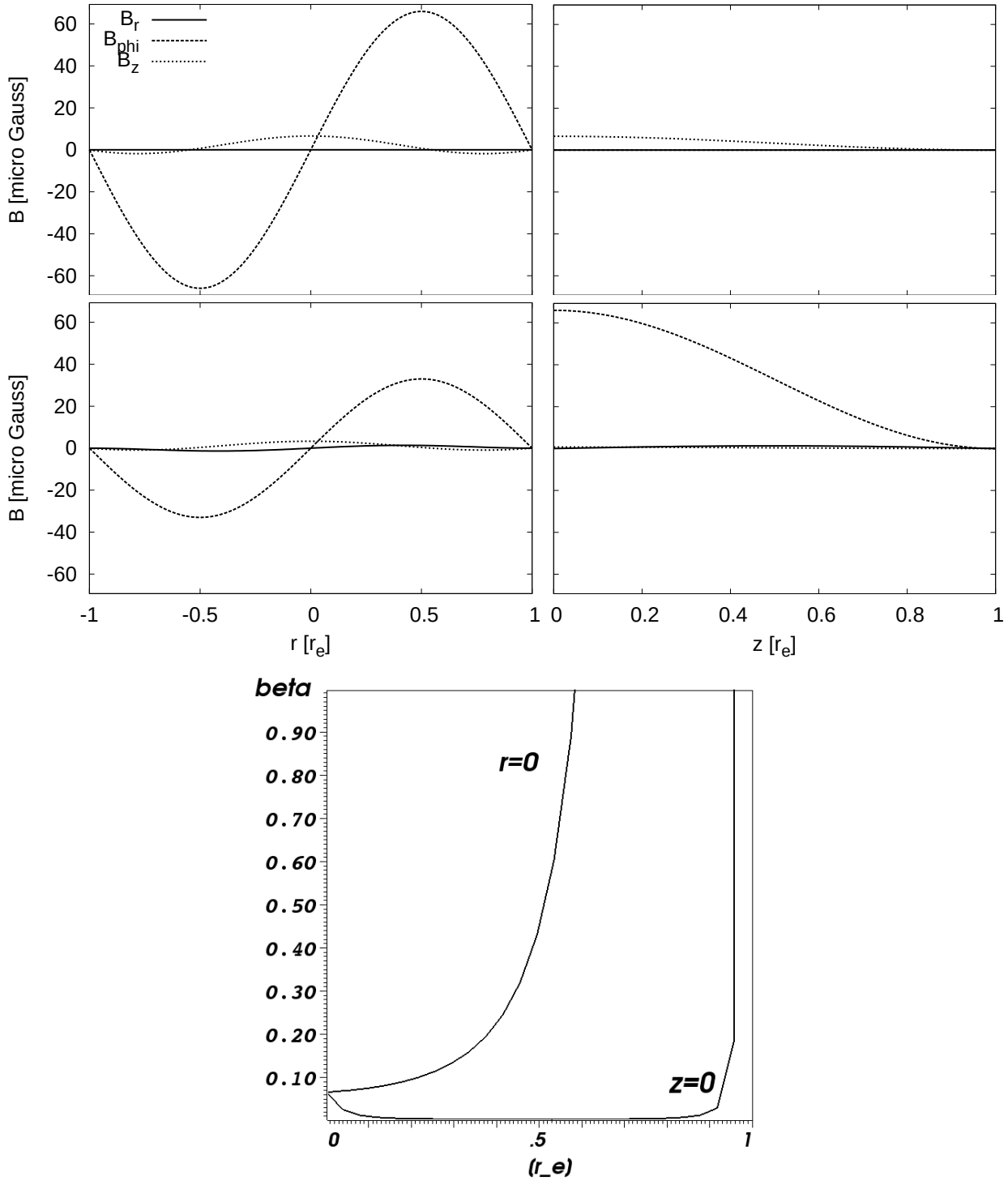

Fig. 1.— Profiles of the initial magnetic components as a function of r and z. $z = 0$ (top left), $r = 0$ (top right), $z = r_e/2$ (middle left) and $r = r_e/2$ (middle right). The initial magnetic beta parameter, **which is the thermal to magnetic pressure ratio (bottom).**

For numerical stabilization we **continually add static gas to grid region within** $r, z < r_e$**. This is done with** the expression

$$\rho^{n+1}(r,z) = \rho^n(r,z) + \rho_c \, |\mathbf{B}(r,z)|^2 \, dt, \tag{8}$$

where $\rho^{n+1}(r,z)$ and $\rho^n(r,z)$ represent the gas densities corresponding to the next and the current timestpes, respectively. The constant factor ρ_c, which has units of $\mathrm{kg\,m^{-3}\,s^{-1}\,T^{-2}}$, was set it to 0.01 computational units. **The added gas is very dilute;** the time average average timestep is of order 10^{-4}. **Thus its contribution to the jet material is negligible.**

2.2.2. Hydrodynamic jets

For these simulations we continuously inject kinetic energy and gas to the cells located at $r < r_e$ and z <0, i.e. within the bottom z boundary. This region is equivalent to the base of the magnetic towers (see above). We impose constant boundary conditions in this region, based on the following three assumptions. Firstly, the collimation of the hydrodynamical jet has already happened at sub-resolution scales. Secondly, the magnetic tower and the hydrodynamic jet have comparable maximum time average propagation speeds,

$$v_j = v_z \approx |\mathbf{B}_{\max}|(4\,\pi\,\rho^0_{\mathrm{amb}})^{-1/2}, \tag{9}$$

where ρ^0_{amb} is the initial grid density of 200 particles per cm^3. Thirdly, the magnetic power and energy flux of the magnetic tower are equal to the power and energy flux of the hydro jet for a fixed area,

$$0.5\rho_j v_z^3 \, a = (|\mathbf{B}|^2/8\pi)\,(|\mathbf{B}|(4\pi\rho^0_{\mathrm{amb}})^{-1/2})\,a, \tag{10}$$

where ρ_j is the jet's density and a $(= \pi r_e^2)$ is the area of the energy injection region. Hence,

$$\rho_j = |\mathbf{B}_{\max}|^2(4\pi v_j^2)^{-1}. \tag{11}$$

To ensure the condition (10) at all times, we set $B_c = 10/(1$ time computational unit) in equation (7).

2.3. Simulations

We carry out four simulations. An adiabatic magnetic tower (the "adiabatic tower"), a hydrodynamical jet (the "jet"), a cooling magnetic tower (the "cooling tower"), and an adiabatic rotating magnetic tower (the "rotating tower"). The first two models have been described in the previous section. The numerical setup of the adiabatic and the cooling towers is the same. Yet, only the cooling case is affected by optically thin cooling which we have implemented using the tables of Dalgarno & McCray (1972) via the source term $\Delta(T)$ in equation (3).

The numerical setup of the adiabatic and the rotating magnetic towers is the same. In the rotating case, however, we continuously give an azimuthal velocity to the central gas and magnetic fields of the tower. This velocity is equal to the Keplerian speed of a two solar mass star:

$$v_\phi = \begin{cases} \sqrt{G2M_\odot/r}, & \text{for } r, z < r_e; \\ 0, & \text{for } r, z \geq r_e. \end{cases} \tag{12}$$

Our choice of two solar masses is arbitrary but within the expected values for proto-stellar and young stellar object (YSO) jets (e.g. see Konigl & Pudritz 2000, and references therein). We note that the gas in our simulations is not affected by any gravitational forces, hence the centrifugal expansion produced by (12) is only balanced by magnetic pressure gradients. We do not expect significant dynamical differences with respect to a case in which gas was affected by gravity; we simulate jets far from the central star (Meier et al. 1997), the magnetic fields are quite strong and the magnetic cavities contain very light gas

(see below).

3. Results

3.1. Plasma structure and evolution

In Figure 2 we show the evolution of the plasma with logarithmic false color density maps. From left to right, columns in the Figure show the adiabatic, the rotating and the cooling magnetic towers, and then the hydrodynamical jet. Time increases downwards, row-wise. Based on the middle row, left-most column panel of Figure 2, we denote the parts of the magnetic towers in the following way, depending on their distance from the jet axis, r: the core (brightest plasma within $r \lesssim 0.4$); the jet (bright plasma within $r \lesssim 1.6$); the magnetic cavity (dark plasma within $1.6 \lesssim r \lesssim 4$, outside the jet) and the contact discontinuity (thin surface between the magnetic cavity and the external medium's brighter plasma). Further out, we see the shocked ambient plasma (bright component, just ahead of the tower's contact discontinuity) and then, at the largest radii, the unperturbed ambient medium plasma.

We see that the initial geometry and strength of the magnetic towers is such that field lines and gas are pushed away vertically from the center. Magnetic cavities with low plasma density are formed. Inside each cavity we see a central cylindrical plasma column which carries a strong current density (section 3.2). A jet is thus driven by rising toroidal magnetic loops. The jets and their corresponding magnetic cavities expand and accelerate, specially along the z-axis. This drives bow shocks on the external unmagnetized media. The radial collimation of the magnetic cavities is caused by the pressure of the external plasma. The jets, on the other hand, are collimated by the magnetic field lines about them (section 3.2). This magnetic tower evolution is consistent with the analytical model of

Lynden-Bell (1996, 2003), as well as with previous simulations of PFD jets and magnetic towers (see e.g. Shibata & Uchida 1986; Nakamura & Meier 2004; Li et al. 2006).

On the other hand, our hydrodynamical jet model is dominated by its axial kinetic energy. Magnetic fields play no role at all in this simulation. We see that the collimated jet produces the basic fluid dynamical structures found in previous simulations of supersonic jets with comparable jet to ambient density ratios (e.g. see Lind et al. 1989; Frank et al. 1998). A strong bow shock is formed in the external medium, behind which a contact discontinuity bounds an unmagnetized cavity that is inflated by the jets former plasma.

By comparing the magnetic towers with the hydrodynamical jet, we find the following (Figure 2). The towers propagate with very similar vertical velocities but decelerate, by about 20%, relative to the hydrodynamical jet. This results because although the towers and the hydro jet have the same injected energy flux, the towers produce not only axial but radial expansion. The pre-collimated hydro jet can only expand via a much lower thermal pressure. Thus all of the energy flux in the hydro-case for our set up is more efficiently directed to axial mechanical power. In principle, our hydro case can emulate the asymptotic propagation regime of a jet that was been magneto-centrifugally launched (e.g. Blackman 2007), which is distinct from a magnetic tower jet. As expected, the towers and the hydro jet show different structures: towers have a thin central jet which is susceptible to instabilities, whereas the hydrodynamical jet's beam is ~ 5 times thicker, smooth and stable. We consistently see lower densities in the towers' cavities than in the one of the hydrodynamical jet. The laboratory experiment magnetic towers of (Lebedev et al. 2005; Suzuki-Vidal et al. 2010) also show the magnetic cavity is mostly void of any plasma. The gas distribution inside the cavities is more complex, and shows smaller-scale structures, in the magnetic tower cases than in the hydrodynamical one.

Amongst magnetic towers, we see they are affected by either cooling or rotation

after their early expansion phase. Instabilities develop in their central jet after $\sim 70\,\mathrm{yr}$ (section 3.3.1). The cocoon geometry of the cooling case (third column from left to right) is the fattest, but the one of the other two cases is very similar. We find that the volume of the ambient region which is affected by the towers is smaller in the cooling case, as expected (e.g. see Frank et al. 1998; Huarte-Espinosa et al. 2011). The above findings allow us to predict very different emission distributions for Poyinting-flux and kinetic-energy dominated jets. **We defer this to a future study.**

The evolution of the magnetic towers' gas density is consistent with that of their compressive MHD and hydrodynamic waves and shocks. In Figure 3 we show profiles of the relevant velocities of the towers (v_x, v_y, v_z, the sound speed and the Alfvén one) along the jets' axis, $r = 0$, as a function of cooling, base rotation and time. During their stable propagation phase, we find that the jets are mostly sub-Alfvénic and trans-sonic, independent of cooling or rotation. Fast-forward compressive MHD (FF) and hydrodynamic **bow** shocks are evident in the ambient medium, ahead of the jets' heads. The FF shocks steepen in time (compare top to middle and middle to bottom rows). The hydrodynamic shocks are quickly dissipated in the cooling case (right column: compare top to middle and middle to bottom rows). In contrast, the adiabatic and rotating cases show regions within the lower half of the jet length where the sound speed is super-Alfvénic. Such regions are bounded by the reverse and the forward slow-modes of compressive MHD waves, and characterised by high thermal to magnetic pressure ratios (section 3.3).

At $t \gtrsim 90\,\mathrm{yr}$ the distribution of waves and shocks of both the rotating and cooling cases (bottom row, middle and right columns) is significantly affected. This is due to the growth of non-linear current-driven instabilities (section 3.3.1). Possibly, pressure driven modes coexist with the current driven ones in regions of high β. We see fast azimuthal velocities, yet mostly sub-Alfvénic, in the central part of these jets.

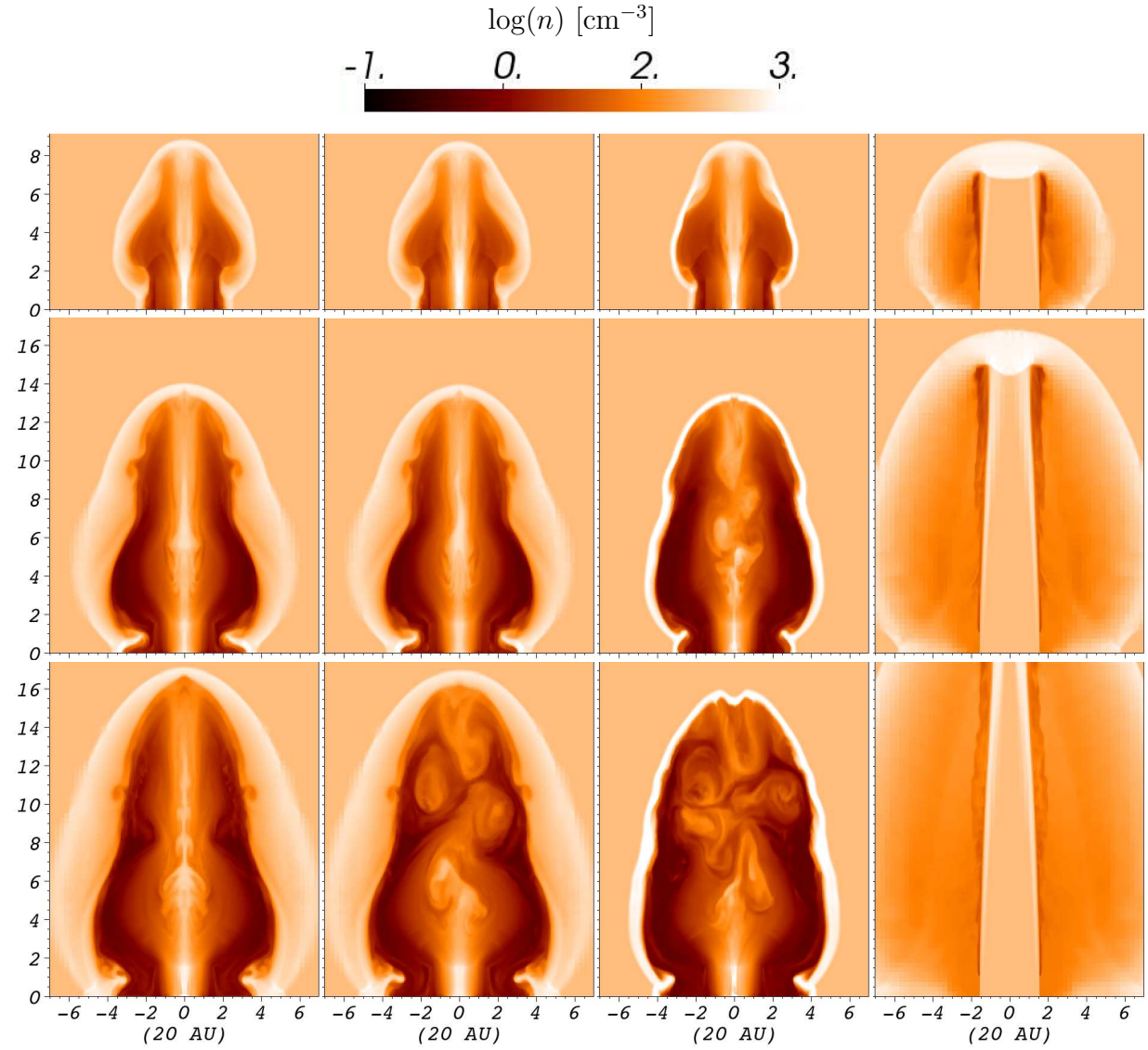

Fig. 2.— Evolution of the plasma gas density. These false color logarithmic maps show the magnetic towers in the adiabatic (1st column), the rotating (2nd column) and the cooling (3rd column) cases, and the hydrodynamic jet (4th column). From top to bottom time is equal to 42, 84 and 118 yr.

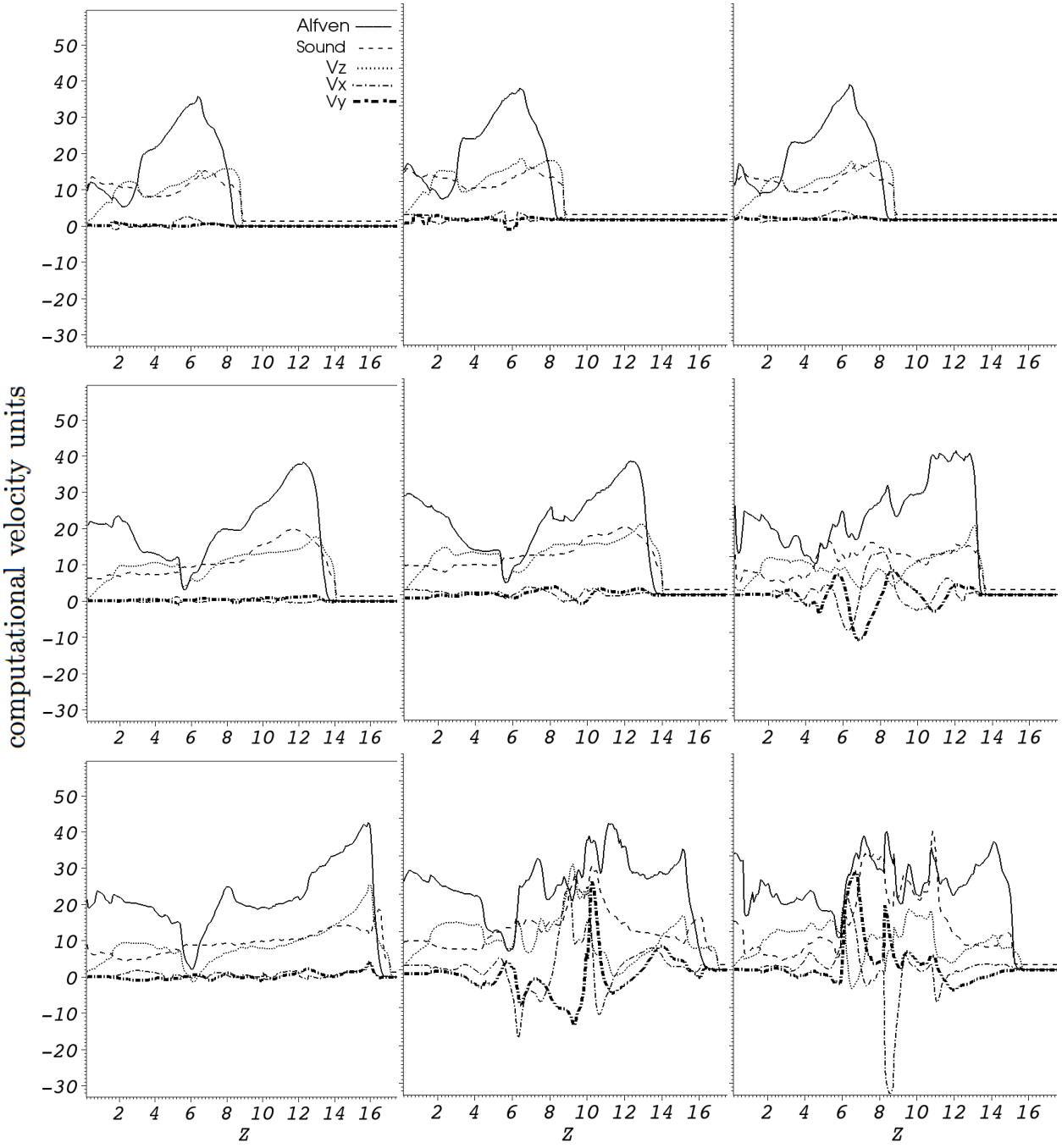

Fig. 3.— Evolution of the plasma velocities along the jets' axis. These are the magnetic towers in the adiabatic (left), the rotating (middle) and the cooling (right) cases. From top to bottom time is equal to 42, 84 and 118 yr. Each computational velocity unit is equivalent to 9.1 $\mathrm{km\,s^{-1}}$.

3.2. Magnetic fields and current density

In Figure 4 we show the distribution of the towers' magnetic fields. These are linear color maps of the absolute value of the toroidal to poloidal field component ratio. From left to right we show the adiabatic, the rotating and the cooling cases, respectively, and time increases downwards, row-wise. We see that the magnetic flux, or the direction of the field lines, consistently changes along the radial direction. In general there are four main nested surfaces or layers of magnetic field lines (e.g. see middle row, left column panel): At the very core we see poloidal fields, B_z. These are surrounded by a surface of toroidal flux. Both of these field components form the jets' plasma columns and are contained within, and collimated by, two outer magnetic surfaces. The small one of these, is dominated by poloidal lines, whereas the large one is dominated by toroidal lines. These outer field lines are collimated by the thermal pressure and inertia of the external media.

As expected, the geometry of the towers' magnetic fields changes in time. Initially, the field lines have a highly wound helical configuration (section 2.1). The magnetic pressure is very high and unbalanced in the vertical direction. The toroidal field lines thus move away from each other and the magnetic towers rise. The injection of magnetic energy, or field lines, is such that it keeps this non-force-free configuration at the base of the tower. Thus "new" field lines push the "old" ones upwards. The latter stretch and expand radially, making way for, and collimating, the jets' new field lines.

After the towers early expansion phase ($t \gtrsim 90\,\mathrm{yr}$), we find, in agreement with the results of the previous section, that the jets of both the cooling and the rotating towers are affected by instabilities (section 3.3.1). The final magnetic structure of the towers is clearer in the field line maps we shown in Figure 5. These are the lines in the central part ($r \lesssim 1.2\ r_e$) of the adiabatic (left), the rotating (middle) and the cooling (right) towers at $t = 118\,\mathrm{yr}$. The top and bottom panels shows the towers edge-on and pole-on, respectively.

The adiabatic case shows quite ordered helical field lines and the strongest jet fields (the red ones) of all the towers. We also see that a bunch of toroidal field lines pile up at the tower's tip. Such concentration of lines causes acceleration of the plasma at the tip of the adiabatic jet to supersonic speeds (see bottom, left panel in Figure 3, $z \approx 15$). In contrast, the cooling tower shows the weakest and most disordered field lines. On the other hand, the middle and right panels show clear differences between the cooling and the rotating cases. The instabilities that develop in these towers are clearer in the rotating case (right column; setion 3.3.1).

The magnetic fields in question are of course related with electric currents. In Figure 6 we show the evolution of the axial current density, J_z (panels in this Figure are arranged as in Figure 4). As expected we see a clear correlation between the distributions of the axial current density and the magnetic field. The jets carry a high axial current (red region) which is contained within a current-free region (white one) at larger radii. The main part of the return current (blue region) moves along the contact surface of the towers' cavity. This forms a closed circulation current system which is consistent with previous simulations of PFD jets (see e.g. Lind et al. 1989; Lery & Frank 2000; Nakamura & Meier 2004; Ciardi et al. 2007) and the magnetic tower laboratory experiments of Lebedev et al. (2005) an Suzuki-Vidal et al. (2010). We note however that both the magnetic field and the current density are strictly localized in our model, i.e. no external media components. This is a novel part of our model.

We see that J_z is also affected by the instabilities that develop in both the rotating and cooling towers after their early expansion phase (bottom row, middle and right columns). The effect is pronounced in the jet and current-free cavity regions. The distribution of the return axial current density is mildly affected. In fact, we see very similar axial return current distributions in the adiabatic and the rotating towers (left and right columns,

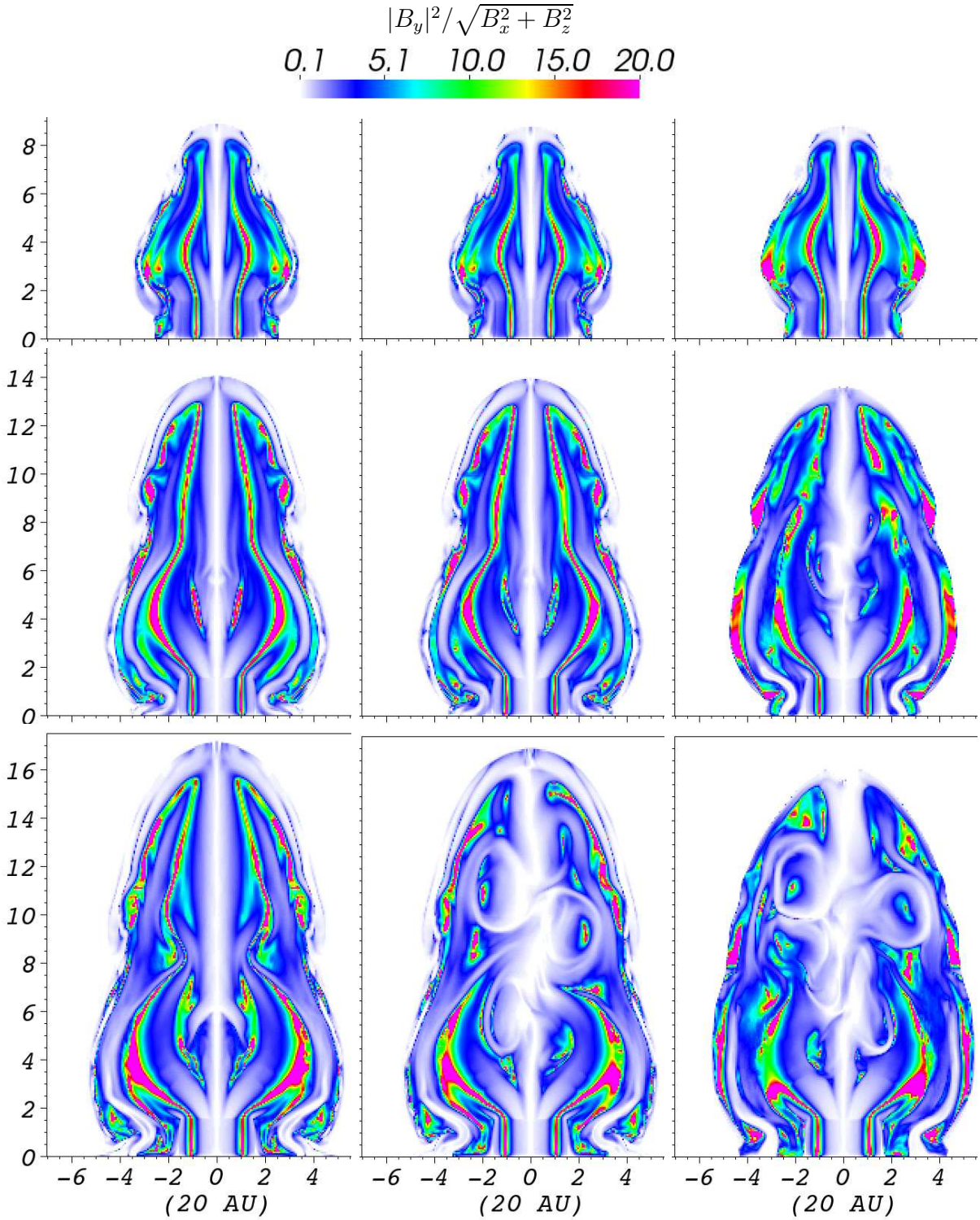

Fig. 4.— Evolution of the towers' magnetic fields. This is the ratio of the toroidal component over the poloidal one. These linear colour maps show the magnetic towers in the adiabatic (left), the rotating (middle) and the cooling (right) cases. From top to bottom time is equal to 42, 84 and 118 yr.

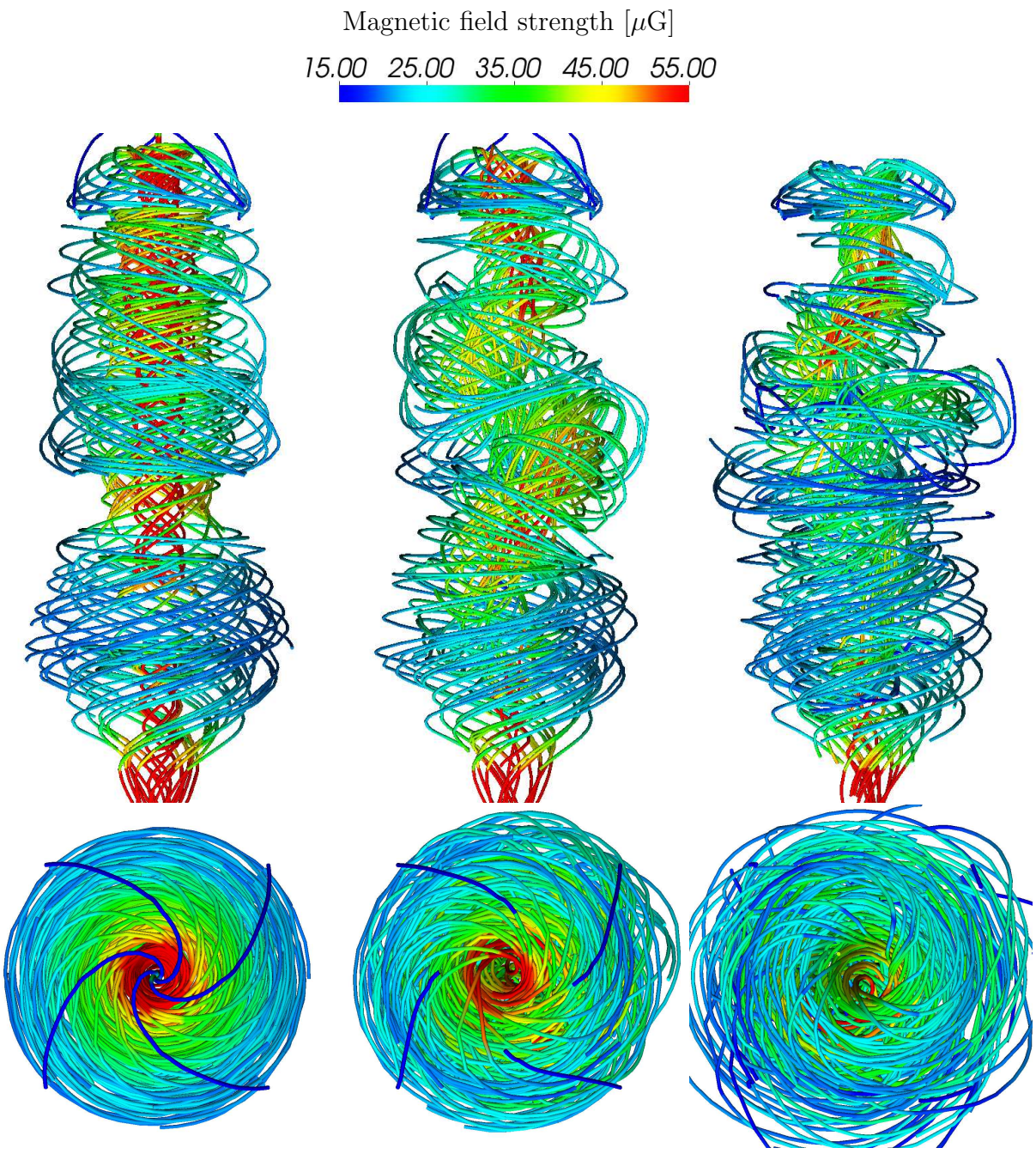

Fig. 5.— Central ($r \lesssim 1.2\ r_e$) magnetic field lines at $t = 118\,\mathrm{yr}$. From left to right these are the adiabatic, the rotating and the cooling magnetic towers, respectively. Bottom panels show an upper view, pole-on. Open field lines are a visualization effect.

respectively), at all times.

3.3. ENERGY FLUX AND FORCES

An interesting open question about magnetized jets is that of the energy flux, both in magnetic and kinetic forms, that the beams carry with them, as well as the relation between this flux and the distance from the jet engine. To study this matter we compute the Poynting flux, f_P, and the kinetic flux, f_k, of out magnetic tower, which are defined as

$$\begin{aligned} f_P &= \oint_s \left[\mathbf{B} \times (\mathbf{V} \times \mathbf{B})\right]_z \, ds, \\ f_k &= \oint_s \tfrac{1}{2}\, \rho \, |\mathbf{V}|^2 \, V_z \, ds. \end{aligned} \tag{13}$$

In Figure 7 we show the distribution of the jets' absolute value of the Poynting to kinetic flux ratio, $\log \left| \frac{f_P}{f_k} \right|$, as a function of time. We note that the area related term of the fluxes cancels in this quotient. These logarithmic maps clearly show that the jets' core is dominated by kinetic energy flux (blue region) while the jets' beam is PFD (red region). A kinetic energy dominated jet core is consistent with the laboratory jets of Lebedev et al. (2005, section 4). Figure 7 clearly shows that the jets of our model magnetic towers are PFD.

Magnetic towers expand due to a combination of magnetic, thermal and inertial forces. In Figure 8 we show the thermal to magnetic pressure ratio, β, using logarithmic greyscale maps (arranged as in Figure 4). As expected for PFD jets we find that the towers' mean beta is well below unity. The adiabatic and rotating cases (left and middle columns, respectively) show regions where $\beta > 1$ and maintain their average position close to $(r, z) = (\,0,\, 6)$. Such regions are located between the reverse an forward slow-mode

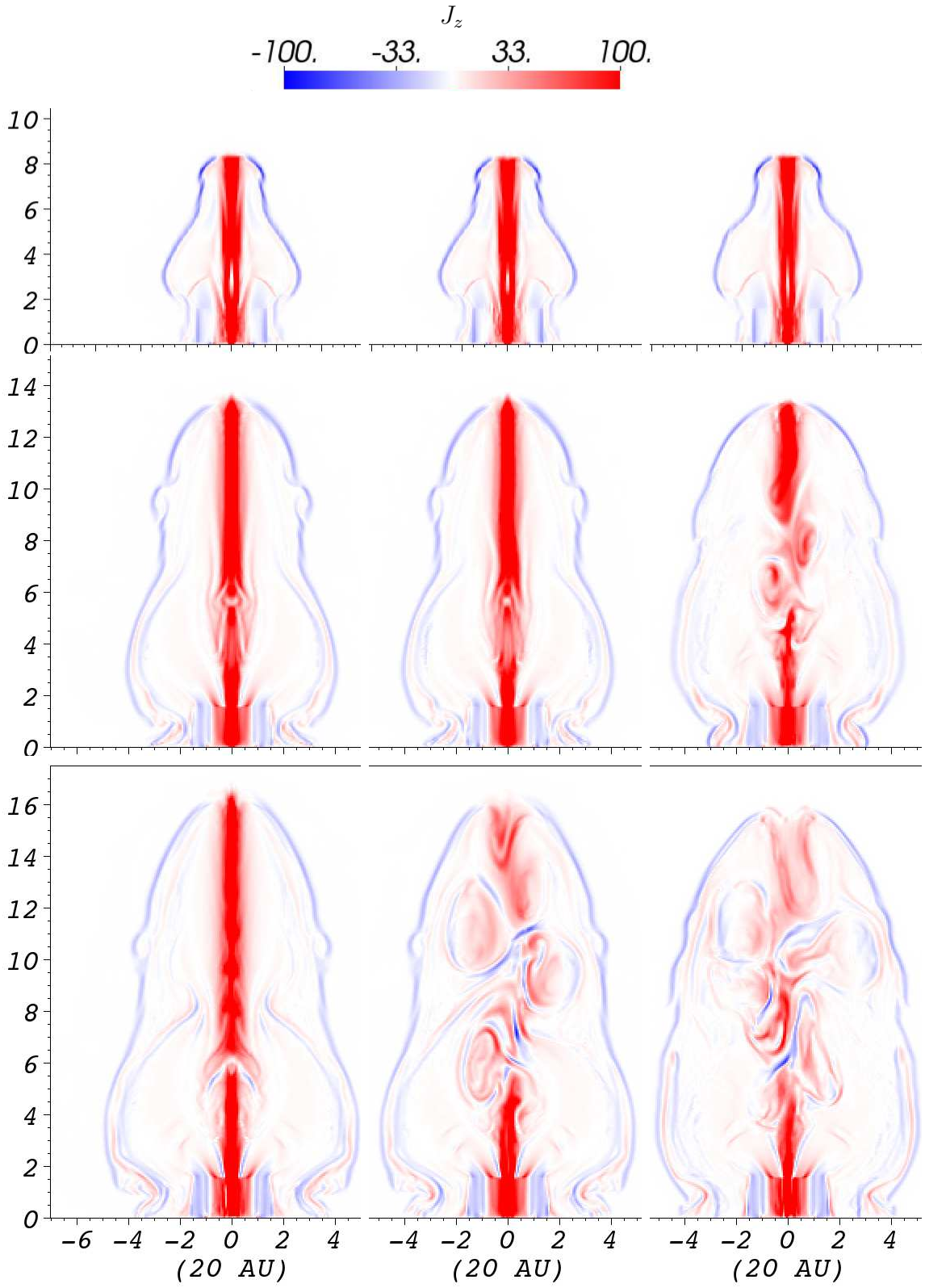

Fig. 6.— Evolution of the axial current density. These linear color maps show the magnetic towers in the adiabatic (left), the rotating (middle) and the cooling (right) cases. From top to bottom time is equal to 42, 84 and 118 yr.

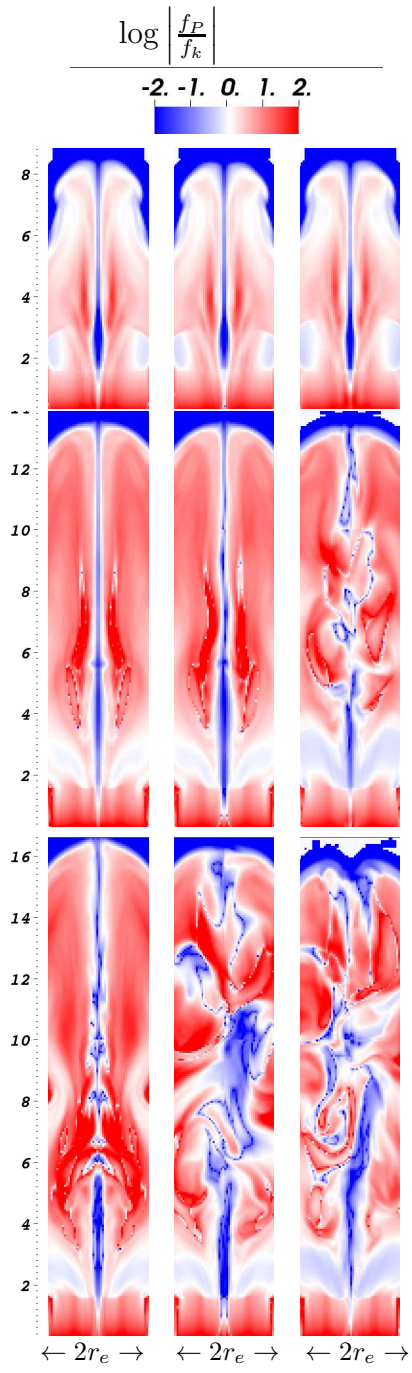

Fig. 7.— Evolution of the ratio of Poynting to kinetic flux. These logarithmic maps show the jets of the magnetic towers in the adiabatic (left), the rotating (middle) and the cooling (right) cases. From top to bottom time is equal to 42, 84 and 118 yr.

compressive MHD waves (Figure 3), and filled with subsonic, weakly magnetized plasma.

It is not surprising that this high-β region is importantly affected by cooling (right column); it reduces the towers' thermal energy. Hence the total pressure of this plasma is dominated by the magnetic component, and it collapses to higher compression ratios than the plasma in the adiabatic limit. Also, in the cooling case, the geometry and topology of the magnetic field in this region changes due to flux freezing and adopts an unstable configuration. Hence the plasma in this high-β region seems to be important for the stability of PFD jets.

In Figure 9 we show the radial component of the forces that are present in the magnetic towers during their intermediate evolutionary phase. These linear color maps clearly show the jet core (colored regions), the central force-free regions (white regions) and the contact discontinuity (outer-most light features, top row) of the towers. In general we see that the inward Lorentz force (top panels) is slightly stronger than both the inertial (or specific centrifugal), $v_\perp^2/x$, and the thermal pressure, $(\nabla P)_x$, forces (bottom panels) which push the plasma outward. The force density distribution responsible for confining the jets and their cavities is clearly shown (along with, e.g., the middle row, left panel of Figures 8 and 6): the jets are confined at the core, where the forward current dominates ($r = 0$, $7 \lesssim z \lesssim 13$). The jets are self-confined in the current-free region located at a few jet radii from the core (i.e. hoop stress). At larger radii near the towers' contact surface, which is also the return current surface (blue outer region in Figure 6), the magnetic pressure is weak and thus it only requires a weak ambient pressure (light-grey outer region, Figure 8) to confine the outer part of the towers.

In section 3.1 we saw that the magnetic towers decelerate with respect to the hydrodynamical jet. This can be explained with the bottom panel in Figure 9, where we see that the magnetic energy that is injected to the towers (within model $r \lesssim 1.5$; section 2.2)

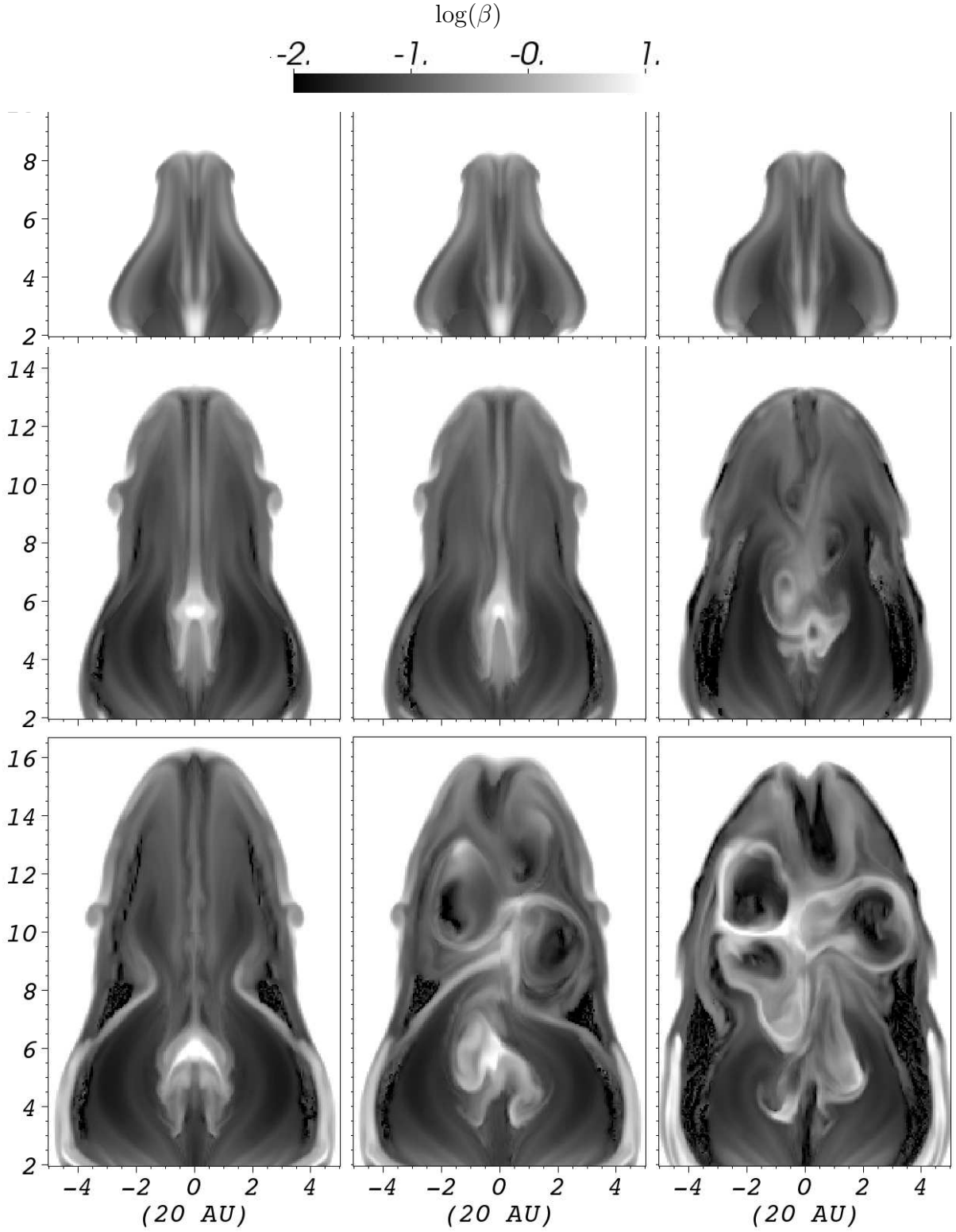

Fig. 8.— Evolution of the thermal to magnetic pressure ratio. These logarithmic greyscale maps show the magnetic towers in the adiabatic (left), the rotating (middle) and the cooling (right) cases. From top to bottom time is equal to 42, 84 and 118 yr.

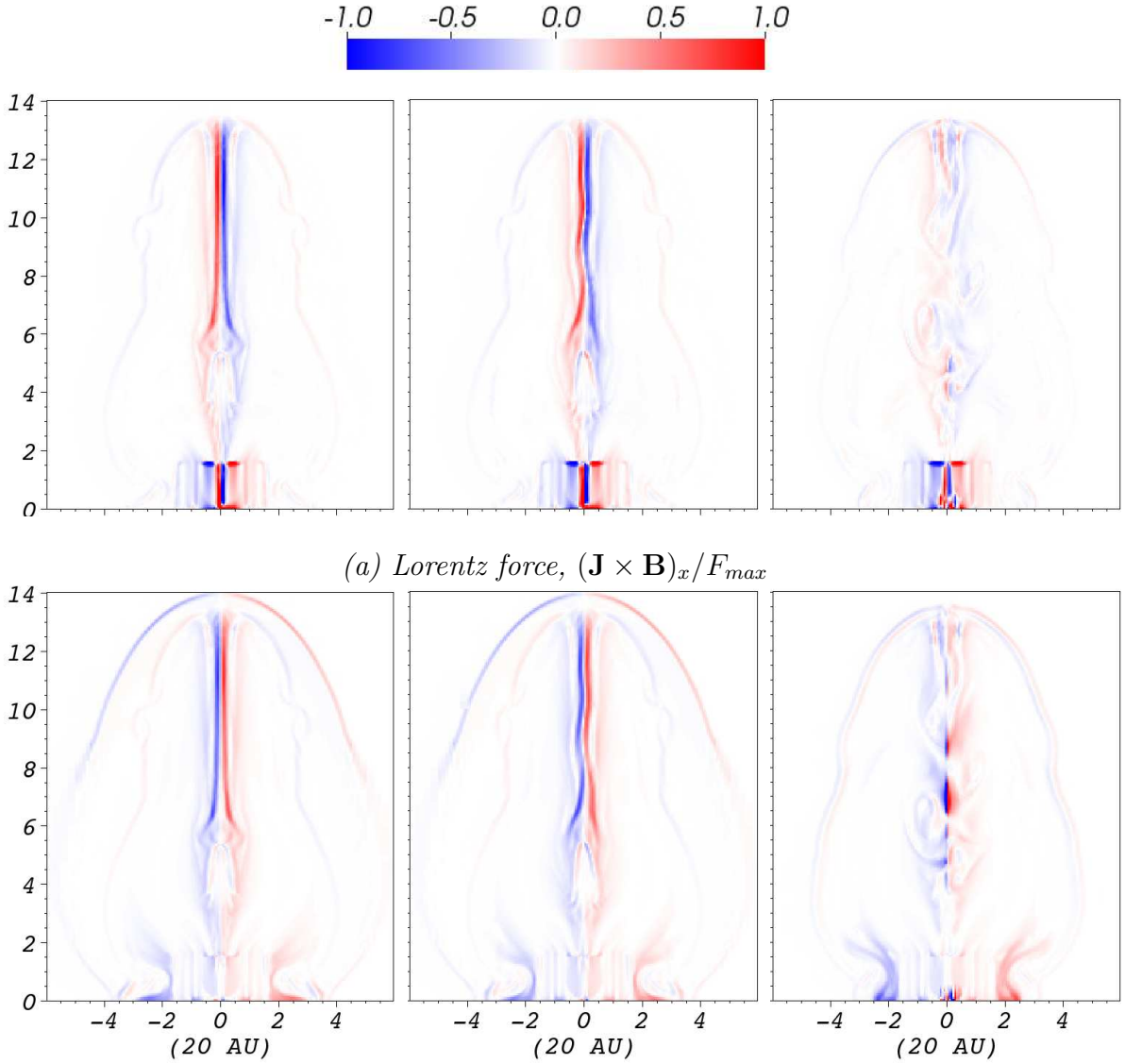

(a) Lorentz force, $(\mathbf{J} \times \mathbf{B})_x / F_{max}$

(b) Inertial force minus the thermal pressure, $(v_\perp^2/x - (\nabla P)_x)/F_{max}$

Fig. 9.— Radial forces at the intermediate evolutionary phase (t = 84 yr) of the towers. Forces are normalized to the maximum value, F_{max}. The horizontal axis is $x = r$, the vertical axis is z and $v_\perp$ is perpendicular to the maps.

causes not only their expected axial (z) expansion, but also their radial expansion via magnetic pressure. In contrast, the kinetic-energy flux that we give to the hydrodynamical supersonic jet is predominantly axial.

3.3.1. Stability

The structure and expansion of our magnetic tower jets are affected by current-driven perturbations. We see evidence of the pinch, $m = 0$, kink, $m = 1$, and $m = 2$ normal mode perturbations. These are expected in expanding magnetized plasma columns and consistent with the models of Nakamura & Meier (2004, and references therein) and Ciardi et al. (2007) – but see also Song & Cao (1983) – and the laboratory experiments of Lebedev et al. (2005) and Suzuki-Vidal et al. (2010). We find that the kink perturbations grow and lead to instabilities in the cooling tower, firstly, and in the rotating one, secondly.

We see that $m = 0$ and 2 perturbations develop in the adiabatic jet after expanding for $\sim 80\,\mathrm{yr}$. These are caused by radial strength gradients in those magnetic fields located outside the jet's core, at the current-free, force-free region. The thermal and both magnetic components of the total pressure balance each others' perturbations locally. As a result, the core of the adiabatic jet adopts the structure of a helical column with an oval-like transverse section, and a lumpy looking longitudinal section (Figure 2) which resembles the projected SII emission distribution of the jet in HH 34 (Reipurth et al. 2002, and references therein). The growth rate of these perturbations is $>120\,\mathrm{yr}$, which in longer than the simulations' final time.

The towers' cores are low beta plasma columns where $|B_\phi/B_z| \ll 1$ (Figure 4). Using perturbation theory we find that their instability condition is given by

$$\left|\frac{B_\phi}{B_z}\right| > |(\beta_z - 1)kr_{jet}|, \tag{14}$$

where $\beta_z = 2\mu_0 P/B_z^2$ and k^{-1} is the characteristic wavelength of the current-driven perturbations. In Figure 3 we see that the cooling jet (right column) shows $\beta_z \sim 1$, or comparable sound and Alfvén speeds, from early in the simulation –see top row $z \sim 2$, middle row $z \sim 5$, and bottom row $z \in$ (6,11). This means that the cooling tower does not have sufficient thermal energy, in comparison with the adiabatic and rotating jets, to balance the magnetic pressure kink perturbations. **In addition, we see that the jet (core) radius, r_{jet}, of the cooling tower is about 20% smaller than that of the adiabatic tower. This is consistent with what is found in laboratory experiments of magnetized supersonic jets, in which outflows with different cooling rates are compared (Ciardi et al. 2012, in prep). Both of these effects (thermal energy losses and core radial compression) reduce the right hand side of (14), hence the kink mode perturbation grow fast and exponentially in the cooling magnetic tower.**

Note that the rotating jet only shows $\beta_z \sim 1$ outside the injection region at $t = 118\,\mathrm{yr}$ (middle column, bottom row). Thus the instability in this case does not arise because of a β effect. Instead, we find that rotation at the base of the tower [equation (12)] causes a progressive, slow amplification of the toroidal magnetic field component of the jet. This is clear in the four panels **at the bottom left part** of Figure 3, where we see that in general the Alfvén speed is higher in the rotating case (middle column) than in the adiabatic one (left column). For this reason, the left hand side of equation (14) increase slowly, and so do the kink mode perturbations. The growth rate of these, is presumably related, in direct proportion, to the mass factor in equation (12); the amplification of the toroidal component at the base of the tower **scales up with** the azimuthal velocity. The rotating jet is not completely destroyed and the amplitude of the kink perturbations is about twice the radius of the central jet column (Figure 5), in agreement with the Kruskal-Shafranov criterion (Kruskal et al. 1958; Shafranov 1958).

A question that naturally arises from the parameter space that we explore here is that of the effect of cooling and rotation on the propagation of our hydrodynamic jet simulation. In addition to the four simulations presented above, we have carried out two variations of the hydrodynamic jet run: one which is affected by thermal energy losses, in the same way as the cooling magnetic tower, and one which has a base ($r < r_e$ and z within the bottom boundary of the computational domain) rotation profile which follows equation (12), as the rotating magnetic tower (section 2.3). The results of the cooling hydrodynamic jet simulation were consistent (as expected) with those found in previous studies (i.e. rather thin jet-produced shocks with high compression factors, see e.g. Frank et al. 1998; Hardee & Stone 1997). Also, we found that the propagation of our hydrodynamic jets was not significantly affected by cooling or rotation relative to the adiabatic case, for the regimes studied.

4. Discussion

The results presented in this paper provide some insight into the evolution of PFD magnetic tower flows. In particular the simulations show new details of the cavity-jet connection, the evolution of the tower given different assumptions (cooling, rotation, etc.) and provide some initial explanation of the stability properties of the central jets which form in the flow.

The applications of our work extend across many classes of collimated astrophysical objects. While we do not explore outflows with relativistic speeds, some aspects of behavior seen in our models can be considered generic. Fragmentation of the central jet, for example, implies that rather than continuous jet beams we should expect high resolution

observations to reveal essentially "clumpy" jets with a distribution of velocities, densities and magnetization. In this way our models can be considered to articulate classes of flow features in AGN radio jets (Tavecchio et al. 2003), X-ray binaries (Miller-Jones et al. 2007) and, perhaps, GRBs (Morsony et al. 2010). **EVERYBODY HAPPY WITH THESE REFERENCES?**

For non-relativistic collimated flows magnetic towers have been proposed as mechanisms for launching some classes of YSO. While the flows downstream at observable distances ($> 10^3$ AU) are clearly kinetic energy dominated, at smaller scales a PFD region may be expected. As Hartigan et al. (2007) have shown, what few measurements of magnetic fields exist in YSO jets indicate there must be a region of sub-alvenic, PFD dominated flow on scales of order 100 AU or less. In addition, these simulations demonstrate (and as laboratory experiments have shown) the long term evolution of magnetic towers may yield a series of collimated clumps whose magnetization properties vary over time. In this way PFD flows may evolve into kinetic energy dominated jets at large distances from the central engine. Planetary Nebula offer another potential application of non-relativistic PFD dominated flows. Magnetic fields are already expected to play an important role in launching pre-Planetary Nebulae (PPN) based on an observed mismatch between momentum in the PPN flow and momentum available through radiation. A number of papers have discussed how strong magnetic fields might create PPN or PN collimated flows (Blackman et al. 2001a,b, Frank & Blackman 2004, Matt, Frank & Blackman 2006, **AF: need others**). Observations of PPN and PN offer morphological similarities to the kinds of features seen in our observations such as hollow lobes and axial clumps. Future work should address these connections.

Of particular importance is the connection between the models presented in this paper and recent "laboratory astrophysic" experiments. These studies utilized Pulsed Power

technologies and were successful in creating high Mach number, fully radiative, magnetized outflows (Lebedev et al. 2005, Ciardi et al. 2007, Ampleford et al. 2008, Ciardi et al. 2009, Frank et al. 2009). The outflows were created when TW electrical pulses (1 MA, 250 ns) are applied to a radial array of fine metallic wires. Lorentz forces ablated plasma from the wires creating an ambient plasma above the array. After the complete ablation of wires near the central electrode, the current switches to the plasma to creates a magnetic cavity with a central jet (i.e. a magnetic tower). The central part of the jet is confined and accelerated by the pressure of the toroidal field. Return current flows along the walls of the magnetic cavity, which is in turn confined by the thermal pressure and by inertia of the ambient plasma. As magnetic cavity expands, the jet becomes detached and propagates away from the source at $\sim$200 km s^{-1}. Instabilities which resemble the kink mode ($m = 1$) develop within the body of these jets fragmenting them into well collimated structures with characteristic axial non-uniformities.

Thus the evolution of magnetic towers in the laboratory show a range of features that are strikingly similar to what is seen in our simulations. This concordance is all the more noteworthy in that our initial conditions were in no way tuned to the experiments and are, in fact, a modified version of what can be found in a number of purely astrophysical studies (e.g. Li et al. 2006). Thus it appears that the laboratory experiments and the simulations support each other, as well as the conclusion that both are revealing generic properties of PFD outflows.

Future work should focus more closely on the links with the laboratory experiments. In particular, issues related to the development of kink mode instabilities, their non-linear resolution and the evolution of clumpy magnetized jets should be explored more fully and in more detail. We leave this for future works.

Regarding the effect of rotation at the base of the jets on their stability, we note that

Moll et al. (2008) have carried out 3-D simulations of magnetocentrifugally driven, conical jets, and found that kink instabilities are stronger when a rigid rotation profile is imposed, in comparison to a Keplerian rotation profile. Rigid rotation seems to induce a shearless magnetic field (Moll et al. 2008). A direct comparison with our calculations must be made carefully though; our initial magnetic configuration has a dominant toroidal component and no radial component, while the initial field setup of Moll et al. (2008) is purely radial. Also, our rotating magnetic tower is continually affected by injection of pure magnetic energy, which is not the case of the conical jets of Moll et al. (2008).

5. Conclusions TO BE UPDATED

Our simulations show that PFD jet beams are lighter, slower and less stable than pre-collimated asymptotically hydrodynamic jets. In practice the latter could represent the asymptotic propagation regimes of magneto-centrifugally launched jets, which are distinct from PFD in that PFD remain PFD out to much larger scales. We find that current-driven perturbations in PFD jets are amplified by both cooling and rotation for the regimes studied: Shocks and thermal pressure support are weakened by cooling, making the jets more susceptible to kinking. Rotation amplifies the toroidal magnetic field which also exacerbates the kink instability. Our simulations agree well with the models and experiments of Shibata & Uchida (1986) and Lebedev et al. (2005), respectively.

Financial support for this project was provided by the Space Telescope Science Institute grants HST-AR-11251.01-A and HST-AR-12128.01-A; by the National Science Foundation under award AST-0807363; by the Department of Energy under award DE-SC0001063; and by Cornell University grant 41843-7012. SL acknowledges support from EPSRC Grant No. EP/G001324/1

REFERENCES

Bacciotti, F., Ray, T.P., Mundt, R., Eisffoel, J., & Solf, J., 2002, ApJ, 576, 222

Blackman, E. G., Frank, A., & Welch, C. 2001, ApJ, 546, 288

Blackman E.G., 2007, Ap&SS, 307, 7

Blandford, R. D., & Payne, D. G. 1982, MNRAS, 199, 883

Blondin, J. M., Fryxell, B. A., & Konigl, A. 1990, ApJ, 360, 370

Carrasco-González, C., Rodríguez, L. F., Anglada, G.,

Carroll-Nellenback, J.J., Frank, A., Shroyer, B., & Ding, C., 2011 (in prep) Martí, J., Torrelles, J. M., & Osorio, M. 2010, Science, 330, 1209

Ciardi, A., et al. 2007, Phys. of Plasmas, 14, 056501

Ciardi, A., Lebedev, S. V., Frank, A., et al., 2011, ApJL, 691, L147

Cunningham A. J., Frank A., Varnière P., Mitran S., & Jones, T. W. 2009, ApJS, 182, 519

Dalgarno A., McCray R. A. 1972, ARA&A, 10, 375

Frank, A., Ryu, D., Jones, T. W., & Noriega-Crespo, A. 1998, ApJL, 494, L79

Hardee, P. E., & Stone, J. M. 1997, ApJ, 483, 121

Huarte-Espinosa, M., Frank, A., Blackman, E., 2011, IAU Symposium, 275, 87

Konigl, A., Pudritz, R. E., 2000, Protostars and Planets IV, 759

Kruskal, M. D., Johnson, J. L., Gottlieb, M. B., Goldman, L. M., 1958, Physics of Fluids, 1, 421

Lery, T., & Frank, A., 2000, ApJ, 533, 897

Lebedev, S. V., et al.(2005), MNRAS, 361, 97

Li, H., Lapenta, G., Finn, J. M., Li, S., & Colgate, S. A. 2006, ApJ, 643, 92

Lind, K. R., Payne, D. G., Meier, D. L., & Blandford, R. D., 1989, ApJ, 344, 89

Lovelace, R. V. E., Li, H., Koldoba, A. V., Ustyugova, G. V., & Romanova, M. M. 2002, ApJ, 572, 445

Lynden-Bell, D. 1996, MNRAS, 279, 389

Lynden-Bell, D. 2003, MNRAS, 341, 1360

Meier, D. L., Edgington,

Miller-Jones, J. C. A., Rupen, M. P., Fender, R. P., et al., 2007, MNRAS, 375, 1087 S., Godon, P., Payne, D. G., & Lind, K. R., 1997, Nature, 388, 350

Mohamed S., Podsiadlowski P. 2007, ASPC, 372, 397

Moll, R., Spruit, H. C., & Obergaulinger, M., 2008, A&A, 492, 621

Morsony, B. J., Lazzati, D., & Begelman, M. C., 2010, ApJ, 723, 267

Nakamura, M., & Meier, D. L. 2004, ApJ, 617, 123

Ouyed, R., & Pudritz, R. E. 1997, ApJ, 482, 712

Pudritz, R. E., Ouyed, R., Fendt, C., & Brandenburg, A. 2007, Protostars and Planets V, 277

Reipurth, B., Heathcote, S., Morse, J., Hartigan, P., Bally, J., 2002, AJ, 123, 362

Shafranov, V. D., 1958, Soviet Journal of Experimental and Theoretical Physics, 6, 545

Shibata, K., & Uchida, Y. 1986, PASJ, 38, 631

Song, M.-T., Cao, T.-J., 1983, Chinese Astron. Astrophys., 7, 159

Suzuki-Vidal, F., Lebedev, S. V., Bland, S. N., et al., 2010, IEEE Transactions on Plasma Science, 38, 581

Tavecchio, F., Ghisellini, G., & Celotti, A., 2003, A&A, 403, 83

Ustyugova, G. V., Lovelace, R. V. E., Romanova, M. M., Li, H., & Colgate, S. A. 2000, ApJ, 541, L21